Stretchable 3D Wideband Dipole Antennas from Mechanical Assembly for On-body Communication

Jia Zhu[a§*], Zhihui Hu[ab§], Senhao Zhang[acd], Xianzhe Zhang[a], Honglei Zhou[e], Chenghao Xing[f], Huaiqian Guo[a], Donghai Qiu[d], Hongbo Yang[cd], Chaoyun Song[g], and Huanyu Cheng[afh*]

[a] *Department of Engineering Science and Mechanics, The Pennsylvania State University, University Park, Pennsylvania 16802, USA*

[b] *School of Logistics Engineering, Wuhan University of Technology, Wuhan 430063, China*

[c] *School of Biomedical Engineering (Suzhou), Division of Life Sciences and Medicine, University of Science and Technology of China, Hefei, 230022, China*

[d] *Suzhou Institute of Biomedical Engineering and Technology, Chinese Academy of Science, Suzhou, 215011, China*

[e] *Institute of Flexible Electronics Technology of THU, Zhejiang, Jiaxing, 314000, China*

[f] *Department of Materials Science and Engineering, Department of Biomedical Engineering, The Pennsylvania State University, University Park, Pennsylvania 16802, USA*

[g] *School of Engineering and Physical Sciences, Heriot-Watt University, Edinburgh EH14 4AS, Scotland, UK, United Kingdom*

[h] *Department of Biomedical Engineering, The Pennsylvania State University, University Park, Pennsylvania 16802, USA*

[§]These authors contributed equally to this work.

[*]To whom correspondence should be addressed. E-mail: jmz5364@psu.edu (J.Z.), Huanyu.Cheng@psu.edu (H.C.)

Keywords: stretchable 3D dipole antennas; mechanical assembly; wideband operation; on-body wireless communication; wearable and bio-integrated electronics

Abstract: The development of wearable/stretchable electronics could largely benefit from advanced stretchable antennas with excellent on-body performance upon mechanical deformations. Despite the recent developments of stretchable antennas based on intrinsically stretchable

conductors, they are often affected by lossy human tissues and exhibit resonant frequency shifts upon stretching, preventing their applications in wireless communication and powering. This work reports a 3D stretchable wideband dipole antenna from mechanical assembly to simultaneously reduce the frequency detuning and enhance on-body performance. The large bandwidth is achieved by coupling two resonances from two pairs of radiation arms, which is well maintained even when the antenna is directly placed on human bodies or stretched over 25%. Such an excellent on-body performance allows the antenna to robustly transmit the wireless data and energy. The design of the 3D stretchable wideband dipole antenna with significantly-enhanced on-body wireless communication performance was validated by an experimental demonstration that features a small difference in the wirelessly received power between the on-body and off-body use. The combination of the mechanically assembled 3D geometries and the coupled mechanical-electromagnetic properties can open up new opportunities in the deformable 3D antennas and other microwave devices with excellent on-body performance and tunable properties.

1. Introduction

Wireless technologies have been an indispensable component in the emerging wearable/stretchable electronics [1, 2] due to their unique roles in wireless data transmission [3-6] and powering [7 8]. The wirelessly obtained real-time sensing data [3-6] can provide on-demand feedback [9] to yield multifunctional wearable/stretchable electronics with a small footprint for biomedicine with translational impacts. Intrinsically stretchable materials (e.g., conductive textiles [10, 11], elastomeric composites [12, 13], and liquid metals [14-16]) have been employed for stretchable antennas. However, it remains challenging for the resulting antennas to achieve excellent performance and robust electromagnetic properties upon large deformations from human bodies, due to low electrical conductivity and difficulty in soldering for integration with commercial off-the-shelf chips. As an alternative solution, the structural design of conventional metals shows great promise in the design and demonstration of flexible/stretchable antennas [17-21] and other RF devices (e.g., low or high RF filter and reflection surface) [21] high efficiency and easy integration.

Because the deformed radiation element leads to a shift in the resonant frequency (i.e., frequency detuning), the radiation performance of stretchable antennas could not be used for reliable wireless transmission of data/energy, limiting their use as strain sensors [12]. Attempts to address this issue include the exploration of a wideband design in stretchable dipole antennas [18] or strain-insensitive stretchable microstrip antennas with a hierarchical structure [19]. The former couples two resonances from two pairs of radiation arms for a large operational band even under deformations, whereas the latter uses the mechanical assembly to generate the 3D hierarchical structure. The wide bandwidth of the antenna also allows it to combine the radiofrequency (RF) energy over its wideband into a usable DC power (with the aid of a rectifier) at a much higher effective conversion efficiency, which is particularly important to harvest the ambient RF energy at typical radio signal levels.

As human tissues with a large water and ion content lead to a high dielectric loss in RF applications, the stretchable antennas exhibit degraded performance in their vicinity. While microstrip patch antennas with a ground layer can effectively reduce the influence from lossy tissues [22], they are more difficult to fabricate, miniaturize, or exhibit wideband properties (for RF energy harvesting). On the other hand, the antennas without a plane structure (e.g., monopole or dipole antennas) can be easily designed and fabricated to exhibit stretchable and wideband

properties. However, they are easily influenced by human tissues, resulting in drastic changes in the working frequency range and other radiation properties when directly attached to the human tissue. In addition, the monopole and dipole antennas in 2D forms have limited stretchability, which may not be sufficient to accommodate the large deformation at varying locations of the skin surface for on-body applications. Although antennas with 3D geometries have been explored (e.g., 3D stretchable monopole antennas [23], 3D dipole antennas with reconfigurable working frequency [24], and controllable electromagnetic shielding [22]), it remains unclear if they can address the above challenges.

In this work, we report a 3D stretchable wideband dipole antenna that is mechanically assembled from a 2D precursor pattern to simultaneously reduce the frequency detuning, improve the stretchability, and enhance on-body performance. Compared to its 2D counterpart that is influenced by a fingertip within 7 mm, the 3D dipole antenna highlights a significantly reduced distance of 1 mm. The further optimized 3D stretchable wideband dipole antenna exhibits a wide operational bandwidth even when it is directly placed on human bodies or stretched over 25%. Compared with its 2D counterpart, the 3D antenna with significantly reduced performance degradation can provide much improved on-body energy harvesting efficiency to enable a self-powered sensing platform. The design that combines the coupled mechanical-electromagnetic properties and 3D geometries from the mechanical assembly can open up new opportunities in the deformable 3D antennas and other RF devices with excellent on-body performance and tunable properties.

2. Results and discussion

The fabrication of the 3D dipole antenna relies on the mechanically guided assembly from 2D planar precursor structures (**Figure 1a**). Briefly, the 2D structure is selectively bonded to a pre-stretched elastomeric substrate at programmable designed locations. The release of the pre-strain generates compressive force to lift the unbonded region to pop out, creating unique 3D structures. In the proof-of-concept demonstration, two pairs of serpentine radiation arms (**Figure S1**) consisting of the same repeating unit fabricated by laser cutting (**Video S1**) have been selected for increased bandwidth due to the coupling effect between the two pairs. The thickness of copper (Cu) of 9 μm in the commercial polyimide (PI)/Cu foil is much larger than its skin depth at the target frequency (1–2 μm), allowing for simple fabrication of radiation arms and high radiation

efficiency. The width of radiation arms also has a negligibly small influence on the radiation performance of the stretchable dipole antenna (**Figure S2**). The feeding at the short arms provides low reflection in the targeting frequency range (**Figure S3**). Besides the level of pre-strain and the geometry of the 2D precursor pattern, the strategic bonding sites between the 2D pattern and the pre-stretched elastomeric substrate also result in different 3D structures. For example, two different 3D coil-like structures are obtained when the bonding sites are selected at full ("3D_full") or half wavelength ("3D_half") (**Figure 1b**). Finite element analysis (FEA) indicates a small strain (0.7%) in the 3D dipole antenna induced by a 15% pre-strain (**Figure S4**). The bonding site at the feeding location in the middle is also encapsulated by the same elastomer (i.e., Dragon Skin) as in the substrate to avoid delamination and electrical disconnection upon stretching. When the 2D pattern is fully bonded to a pre-stretched elastomer with lower stiffness (Ecoflex), the strategy of pre-strain can generate in-plane bending and limit out-of-plane buckling in the serpentine arm, creating a "rippled" dipole antenna. It should be noted that the 3D antenna from mechanical assembly with selective bonding sites degenerates to its 2D counterpart with the same selective bonding when the pre-strain is vanishing.

Coupled mechanical-electromagnetic properties of stretchable 3D dipole antennas

The coupled mechanical-electromagnetic properties of the stretchable 3D dipole antennas are obtained by investigating the radiation performance of the antenna at different strain levels. Though the serpentine arms in the 2D dipole antenna bonded at the full-wavelength locations can unfold in the plane upon stretching, the stretchability of the antenna is only ~ 10%. In contrast, the applied pre-strain in the 3D dipole antenna allows it to first flatten the 3D structure and then unfold the serpentine arms (**Figure 2a**), which provides improved stretchability. Because of the ordered unraveling, the stretchability of the 3D dipole antenna is approximately the sum of the pre-strain and the stretchability of its 2D counterpart. Therefore, the "3D_full" dipole antenna induced by a 15% pre-strain exhibits an improved stretchability of 25%. However, it is important to note that the stretchability of the 3D antenna also depends on the location and number of bonding sites, because the serpentine elements bonded at these locations would have limited stretchability. As a result, the "3D_half" dipole antenna with more bonding sites than that of the "3D_full" dipole antenna shows a smaller stretchability of 20%.

The large bandwidth of the capacitively coupled 2D dipole antenna comes from the coupling of two distinctive resonances contributed by the parasitic (long) and driven (short) arms (**Figure 2b**). While the tensile strain applied to the antenna leads to the unfolding of serpentine arms and shifts of the two resonances to lower frequency values, the shift is much smaller than the bandwidth (frequency range with S_{11} values lower than -10 dB). As a result, the 2D dipole antenna exhibits a large operational band of 0.44 GHz in the tensile strain range from 0 to 10 % (the highlighted region in **Figure 2b**). Despite the change in the relative position between the two pairs of serpentine arms, the 3D dipole antenna ("3D_full" or "3D_half") also showcases the dual-resonance characteristic (**Figure 2c** and **d**). In theory, the resonant frequency of a straight dipole antenna can be approximately expressed as $c/(2L\sqrt{\varepsilon_r})$, where c is the speed of light in vacuum, L is the half-length of the dipole antenna, and ε_r is the effective dielectric constant. The air gap between the serpentine arms and dielectric substrate in the 3D dipole antenna leads to a decreased effective dielectric constant and, thus, a higher resonant frequency than its 2D counterpart. Compared with the two resonances (2.14 and 2.34 GHz) of the undeformed 2D dipole antenna, the "3D_half" (or "3D_full") dipole antenna shows slightly increased resonances to 2.31 and 2.68 GHz (or 2.27 and 2.70 GHz). Similar to the 2D dipole antenna, the 3D dipole antenna upon stretching also shows a shift of the S_{11} curve to a lower frequency. In particular, the higher resonant frequency of the 3D dipole antenna from the short (driven) arm (indicated by the arrow in **Figure 2b-d**) decreases with the tensile strain in an approximately linear manner (**Figure 2e**).

Despite the existence of the "dual-resonance" characteristic, the 3D dipole antenna directly transformed from its 2D counterpart induced by a 15% pre-strain does not show a large bandwidth due to the high reflection -at the lower resonant frequency (i.e., > -10 dB). The change of arm structures and effective dielectric constant in the "3D_full" dipole antenna leads to the impedance change from (43-12i) to (54-53i) Ω, resulting in a large deviation from (50+0i) Ω degrades. As a result, the S_{11} value of the "3D_full" dipole antenna at the lower resonant is only around -7.0 dB. The issue of poor impedance matching to the 50 Ω port is more evident in the "3D_half" dipole antenna. The S_{11} value of the "3D_half" dipole antenna at the high resonance is merely -13.0 dB, which is much larger than -31.0 dB for the 2D dipole antenna. The entire S_{11} curve of the "3D_half" dipole antenna upon 20% stretching even shifts above the -10 dB line (**Figure 2d**), which results in a vanishing operation band upon stretching. In comparison, the "3D_full" dipole antenna shows

a larger stretchability and better impedance matching. Realizing the full potential of the 3D dipole antenna relies on further optimization of its radiation performance, which can be simply achieved by modulating its geometry of the 2D pattern such as the length of radiation arms for reduced reflection coefficient (**Figure S5**). For example, increasing the actual length of the short (driven) arm by 1 mm significantly improves the overall impedance matching for the "3D_full" dipole antenna (**Figure 2f**). The resulting optimized "3D_full" dipole antenna exhibits the increased operational bandwidth upon stretching from 0.12 GHz to 0.21 GHz by 75%. The operational bandwidth upon stretching also covers the common target frequency of ~ 2.45 GHz for wireless communication and ambient RF energy harvesting. Despite the reduced operational bandwidth upon stretching, the stretchable 3D dipole antenna provides much larger overall stretchability and improved on-body radiation efficiency (see the following discussion), which is more critical for wearable applications. The optimized "3D_full" dipole antenna is chosen in the following discussion unless specified otherwise. On the other hand, reducing the actual length of the short arm by 1 mm leads to further separation between two resonances and increased reflection at the lower resonance, which does not increase the operational band. It is realized that the separation between the two resonances has a profound influence on the overall impedance matching and resulting bandwidth. It should be noted that other geometric parameters (e.g., the serpentine arc unit and the gap between two pairs) [18] can also be optimized to tune the stretchability and radiation properties (e.g., the target frequency and bandwidth) of the 3D dipole antennas. The 3D dipole antenna bent over varying radii of curvature also shows a small shift in S_{11} curves (**Figure S6**). In addition, the negligibly small variations in the S_{11} curve of the optimized 3D dipole antenna over cyclic stretching of 5000 times confirm the reliable cyclic performance (**Figure S7**). Since 3D structures can be vulnerable to external forces/pressures, it is also important to investigate the influence of the pressure on the mechanical and electromagnetic properties of the 3D dipole antenna for practical applications. The arch of the 3D dipole antenna can be locally deformed by an external force, but it quickly recovers as the force is removed (**Figure S8a**). The S_{11} curve also exhibits negligibly small changes for the external force from 0 to 20 N (**Figure S8b**). These results are attributed to the local deformation and the relatively small maximum strain of ~ 0.65% in the PI/Cu film that is below the yield strain of Cu (~ 0.7%) (**Figure S8c**). To further protect the 3D structure from the larger global deformation, the 3D stretchable dipole antenna can be placed inside an Ecoflex cavity to avoid mechanical damages without changing its S_{11} curve (**Figure S9**).

Reduced effect of lossy human tissues on the 3D dipole antennas

The large content of water and ions in human tissues would significantly degrade the antenna performance if the antenna is brought close to the human skin [25]. The effect of the lossy human finger on the 3D dipole antenna is first investigated (see the inset in **Figure 3a**) before it can be applied for various on-body applications. After placing a fingertip on top of the 2D dipole antenna at a distance of 1 mm, the "dual-resonance" characteristic disappears and the target frequency of 2.4 GHz also shifts out of the operational band even before the tensile strain is applied (**Figure 3a**). The "dual-resonance" characteristic only begins to recover when the gap distance is increased to ~ 7 mm. In contrast, the influence of the human fingertip is significantly smaller on the "3D_full" and "3D_half" dipole antennas before optimization (**Figure 3b** and **c**). Besides the smaller change in the bandwidth, the "dual-resonance" characteristic almost recovers at a gap distance of 3 mm for both the "3D_full" and "3D_half" dipole antennas induced by a 15% pre-strain, which is much smaller than that for their 2D counterpart. The much smaller influence of human tissues on the 3D dipole antenna mainly originates from the smaller shift of S_{11} curves in the higher frequency range (marked by arrows). The effective dielectric constant of a composite can be expressed as $\varepsilon_f = \sqrt{\frac{\varepsilon_1 f + \varepsilon_2(1-f)}{f/\varepsilon_1 + (1-f)/\varepsilon_2}}$, where ε_i (i = 1 or 2) is the dielectric constant of each component and f is the volume fraction of the 1st component [26]. It can be concluded that the effective dielectric constant of composites is largely determined by the component with a lower dielectric constant since the dielectric constant is weighed by its inverse [26]. The introduction of a low-dielectric air gap in the 3D dipole antenna helps stabilize the effective dielectric constant and S_{11} curve even in the vicinity of human tissues.

As the optimized "3D_full" dipole antenna already shows a much larger operational band than the one before optimization in the air even upon stretching, it is of high interest to investigate its performance in the presence of human fingers or bodies. In the close proximity of 1 mm to human fingers, the optimized "3D_full" dipole antenna shows well-maintained "dual-resonance" characteristic and a slight change in the S_{11} dip magnitude (~ 0.5/8 dB at the lower/higher resonance) (**Figure 3d**). Since the S_{11} value is kept below -10 dB in the target frequency range, a wide operational band of 0.51 GHz, and thus excellent on-body performance, is maintained in the optimized "3D_full" dipole antenna. Since the S_{11} value is kept below -10 dB in the target

frequency range, a wide operational band of 0.51 GHz, and thus excellent on-body performance, is maintained in the optimized "3D_full" dipole antenna. The optimized "3D_full" dipole antenna recovers to its 2D form upon stretching of 15% and approximately follows the deformation of its 2D counterpart upon further stretching to 25%. As a result, the influence of the finger (or human tissues) becomes stronger with the increasing tensile strain (**Figure S10**), indicating the important role of 3D structures in improved on-body radiation performance.

Because the level of pre-strain changes the shape of the 3D dipole antenna, it is worthwhile to investigate its influence on the air gap, impedance matching, and radiation performance. As the pre-strain is increased from 5 to 10 and then to 15% (**Figure 4a**), the maximum height of the 3D structure in the "3D_full" dipole antenna is measured to increase from 1.9 to 2.3 and then to 2.6 mm (**Figure 4b**). The increase of the pre-strain from 5 to 10 and then to 15% also results in the increased two resonant frequencies from 2.25/2.56 GHz to 2.27/2.67 GHz and then to 2.31/2.68 GHz. Similar to the case of the 15% pre-strain, the "dual-resonance" characteristic of the "3D_full" dipole antenna with a pre-strain of 5% (**Figure 4c**) or 10% (**Figure 4d**) also recovers when the gap distance between the fingertip and antenna is larger than 3 mm. The "on-body" operational band of the "3D_full" dipole antenna induced by 10% pre-strain is larger than that induced by a 5% pre-strain due to the high reflection coefficient at the lower resonant frequency. However, the shift of S_{11} curves of the "3D_full" dipole antenna induced by a 5% or 10% pre-strain to the smaller frequency upon stretching and a high reflection at the lower resonance result in a diminishing operational band due to poor impedance matching (**Figure S11a** and **b**). Increasing the pre-strain level to 30% leads to a higher stretchability (~ 40%) without compromising the operational bandwidth (**Figure S11c**). However, the antenna induced by a 50% pre-strain shows degraded bandwidth due to poor impedance matching (**Figure S11d**). The above observations for the operational band of the "3D_full" dipole antenna also hold for the "3D_half" dipole antenna induced by a 5% or 10% pre-strain (**Figure S12 and S13**). The "3D_half" dipole antenna induced by a 10% pre-strain exhibits a larger on-body operational band of 0.49 GHz (**Figure S12b**) than that of 0.36 GHz induced by a 15% pre-strain before stretching. However, its operational band almost vanishes upon 20% stretching (**Figure S13b**), which is significantly smaller than that of 0.12 GHz induced by a 15% pre-strain.

Compared with the "3D_full" dipole antenna induced by the pre-strain of 15%, the rippled dipole antenna from the same selective bonding and pre-strain level shows a similar stretchability of 25% and two resonant frequencies (2.33 and 2.66 GHz) (**Figure S14**). However, the operational band of the rippled dipole antenna diminishes upon stretching. The "dual-resonance" characteristic in the ripple dipole antenna only recovers when the gap distance between the fingertip and antenna becomes larger than 7 mm. The results imply that the 3D structure is the major factor that contributes to the improved on-body radiation performance of the stretchable 3D dipole antennas.

On-body wireless communication and RF energy harvesting of 3D dipole antennas

Compared with the 2D or rippled dipole antennas, the optimized 3D dipole antenna with the drastically reduced influence from the lossy human tissues is promising for on-body wireless communication and RF energy harvesting. As an example, the on-body wireless communication of the optimized "3D_full" dipole antenna induced by a 15% pre-strain has an operational band to cover the commonly used Bluetooth and Wi-Fi (2.40 - 2.48 GHz), which is suitable for wireless transmission of data and energy. After attaching the "3D_full" dipole antenna to the human arm by a Silbione adhesive layer (**Figure 5a**), the "dual-resonance" characteristic still exists (see the mark in **Figure S15a**), whereas the one in the 2D dipole antenna disappears (**Figure S15b**). Notably, the optimized "3D_full" dipole antenna on the human arm still exhibits a large operational bandwidth of 0.22 GHz in the large stretching range from 0 to 25%.

The wireless communication of the 3D dipole antenna is evaluated with a commercial RF kit that includes a transmitter and receiver pair (SmartRF06) (**Figure 5b**). Consisting of the stretchable dipole antenna and a CC2538 RF chip, the transmitter can be programmed to transmit RF power of -3 dBm (0.50 mW) at ~ 2.45 GHz. An omnidirectional monopolar antenna is integrated with the receiver that has a sensitivity of -100 dBm. In the open space at a university campus, the communication performance of the stretchable 2D (**Figure S16**) and 3D dipole antenna (**Figure 5c**) on the human skin before and after stretching is compared with that in the air. The received power decreases with the communication distance between the transmitter and receiver up to ~ 70 m (**Figure 5d**), which can be further increased with a higher transmitting power. Compared with the previously reported stretchable monopole antenna to receive - 75 dBm at a

distance of 20 m from a 1 dBm power source in the free space [27], the optimized "3D_full" dipole antenna only needs a power source of -3 dBm, which saves the energy of more than 60%. The optimized "3D_full" antenna also exhibits a significantly enhanced on-body performance over the 2D dipole antenna, manifested by the smaller difference in the received power between the on-body and off-body use (termed as on-body degradation) (**Figure 5e**). At a distance of 1 m, the on-body degradation in the optimized "3D_full" antenna is only 3 dB, which is much smaller than that of 16 dB in the 2D counterpart (**Figure S16**). This degradation is even comparable to that of 3 dB from the stretchable microstrip patch antenna that is known for good on-body performance [19], showcasing the excellent on-body performance of the "3D_full" dipole antenna. The measured radiation pattern of the "3D_full" dipole antenna also shows a higher front-to-back ratio of 3.2 dB (more radiation along +z direction) than that of 1.1 dB from its 2D counterpart likely contributed by the air gap from the 3D structure (**Figure S17**). The preferred radiation along the +z direction helps reduce the influence of lossy tissues underneath the radiation part. When used as a receiver, the 3D dipole antenna also exhibits excellent on-body wireless communication performance due to the reciprocity principle (**Figure S18**). Consisting of an antenna and a rectifier, the rectifying antenna (or rectenna) can harvest the RF energy into usable DC power. By leveraging our recent work on stretchable rectennas [18], the optimized "3D_full" antenna with large operational bandwidth and excellent on-body performance can drastically boost the energy harvesting efficiency in the resulting stretchable rectenna on the skin. In a proof-of-concept demonstration, the stretchable 3D dipole antenna can efficiently harvest RF energy to power a red light-emitting diode (LED) (**Figure 5f**). The integration of the RF energy harvesting module with a stretchable strain sensor based on laser-induced graphene (LIG) further yields a self-powered sensing platform for continuous pulse measurements (**Figure 5g**). It should be noted that the same strategy also applies to a smaller stretchable dipole antenna (20.1 mm by 1.8 mm) working at a higher frequency (~ 5 GHz) (**Figure S19**), which facilitates the integration in practical applications.

3. Conclusion

In summary, this work reports the design and demonstration of a new class of stretchable 3D dipole antennas by the versatile approach of mechanical assembly. Compared to its 2D counterpart, the mechanically assembled 3D dipole antenna allows ordered unraveling to provide improved

stretchability. More importantly, 3D dipole antennas with the "dual-resonance" characteristic provide a large operational band even upon stretching, which is highly desirable for stable wireless communication and RF energy harvesting. Real-time on-body wireless communication further confirms the excellent performance of the 3D dipole antenna. The design guidelines for the 3D dipole antenna can also be applied for the other wearable wireless communication modules.

Experimental sections

Fabrication of 2D/3D dipole antennas

After laminating the PI/Cu foil (9/12 μm) on the silicon wafer coated with a thin 10:1 PDMS layer, the foil was patterned into serpentine traces by a 1065 nm fiber laser (20W EP-S, SPI lasers Inc.) according to the design prepared by the Auto CAD software. Next, a soft substrate (Ecoflex or Dragon Skin) with a thickness of 1 mm was prepared by mixing part A with B (1:1 ratio), followed by curing at room temperature for 2 hours. The cured elastomeric substrate was stretched to a prescribed level (5%, 10%, or 15%) by a custom-built stretcher. Created by a 10.6 μm CO_2 laser (VL S2.30, Universal Laser Systems Inc.), the PI masks (50 μm) to define the bonding sites allow the silicone gel to be sprayed at the openings of the mask. With a thermal release tape, the patterned Cu/PI serpentine traces were transferred onto the pre-stretched substrate. After curing the silicone gel (Dragon Skin) to create the strong bonding between the foil and the substrate at desired locations, heating the thermal release tape to 100 ºC led to its removal. The release of the pre-strain generated compressive force and lifted the unbonded serpentine Cu/PI traces to deform out-of-plane for mechanical assembly of 3D dipole antennas. The 2D dipole antenna as a comparison was directly fabricated by using the elastomeric substrate without the pre-strain. After soldering the coaxial cable to the feeding port of dipole antennas, a thin encapsulation layer (Dragon Skin) was applied at the soldering location to avoid delamination upon stretching.

Optimization of the electromagnetic properties of the 2D/3D dipole antennas by simulations

The antenna performance (e.g., reflection curve and radiation pattern) was simulated by the ANSYS high-frequency electromagnetic field simulation (HFSS) package. Tetrahedron elements with automatic and adaptive meshing were adopted to achieve convergence (maximal delta S less than 0.02) within up to 15 passes. The feeding location was chosen at the short arm of the 2D dipole antenna for good overall impedance matching and low reflection in the S_{11} curves.

Following our previous work [18], the length of the short (driven) arms (indicated by the scissor location in **Figure S1**) was optimized to tune the difference between the two resonances and impedance matching for large bandwidth. The 3D dipole antenna was fabricated based on the optimized 2D dipole antenna. Further optimization on the actual length of short arms (i.e., increased or decreased by 1 mm) in the 3D dipole antenna yields the optimized 3D dipole antenna covering the target frequency of 2.45 GHz.

Measurement of the electromagnetic-mechanical properties of 2D/3D dipole antennas

The tensile strain on the stretchable dipole antenna was applied by a custom-built stretcher. The reflection (S_{11}) curves of the antenna before and after stretching were measured by a network analyzer (Keysight E5071C). The radiation pattern of the 2D or 3D dipole antenna was measured in an anechoic chamber.

On-body performance measurement of 2D/3D dipole antennas

Stretchable dipole antennas were fixed on a custom-built stretcher without strain. S_{11} curves were measured with a fingertip placed on the top of dipole antennas at different distances. The on-body performance of the antenna was measured by attaching it to the arm of a healthy human subject with a Silbione adhesive layer.

Wireless communication and energy harvesting performance of 3D dipole antennas

The commercial RF evaluation kit (SmartRF06, Texas Instruments) was employed to measure the wireless communication performance of the stretchable 2D or 3D dipole antenna. Two boards integrated with the CC2538 RF chip acted as the transmitter and receiver, respectively. The chip in the transmitter could be programmed to transmit the RF energy at a power of -3 dBm (0.501 mW). The stretchable dipole antenna was connected with the transmitter as an RF source. The receiver was integrated with a PCB-based omnidirectional monopolar antenna to wirelessly communicate with the transmitter. The receiver was programmed to have a sensitivity of -100 dBm. The received power at different distances for the stretchable dipole antenna placed in the free space or on the human skin was then measured. The LIG-based stretchable strain sensor was prepared by scribing on PI films with a CO_2 laser (power: 10%, speed: 11%, PPI:1000), followed by smearing Dragon Skin precursors on it with a ratio of 1:1. After cured, LIG patterns were peeled off with Dragon Skin substrates. Connecting it with copper wires by silver pastes completes the

fabrication of the stretchable strain sensor. A RF transmitter (10dBm, WB-SG1, WuTong Electronics) combined with a amplifier (20W, EST20, ZhongShi Tech.) was used in RF energy harvesting to ensure the energy output.

Supporting Information

Geometric parameters of the 2D stretchable wideband dipole antenna (Figure S1); Simulated S_{11} curves of the stretchable 2D dipole antennas with different widths of radiation arms (Figure S2); Simulated S_{11} curves and impedance of the stretchable 2D dipole antenna with feeding at the short or long arm (Figure S3); Strain distribution of the "3D_full" dipole antenna induced by a 15% pre-strain (Figure S4); Simulated S_{11} curves of the "3D_full" dipole antenna with different short arm lengths (Figure S5); Measured S_{11} curves of the stretchable 3D dipole antenna bent over varying radii of curvature (Figure S6); Measured S_{11} curves of the stretchable 3D dipole antenna under cyclic stretching of 25% over 5000 times (Figure S7); Mechanical-electromagnetic properties of the stretchable 3D dipole antenna subjected to the external force/pressure (Figure S8); Encapsulation of the stretchable 3D dipole antenna (Figure S9); Measured S11 curves of the stretchable 3D dipole antenna upon the tensile strain of 0%, 15%, and 25% with (dashed lines) or without (solid lines) the fingertip placed at a distance of 1 mm (Figure S10); Mechanical-electromagnetic properties of the stretchable 3D dipole antenna induced by a pre-strain of 5%, 10%, 30%, or 50% (Figure S11); On-body radiation performance of the "3D_half" dipole antenna induced by a pre-strain of 5% or 10% (Figure S12); Mechanical-electromagnetic properties of the "3D_half" dipole antenna induced by a pre-strain of 5% or 10% (Figure S13); Mechanical-electromagnetic properties and on-body radiation performance of the "ripple" dipole antenna induced by a 15% pre-strain (Figure S14); Radiation performance of the stretchable 3D and 2D dipole antennas attached to human arms and upon maximum stretching for each (i.e., 25% for 3D or 10% for 2D antennas (Figure S15); Measured received power by the stretchable 2D dipole antenna in free space, on human arms, or being stretched by a tensile strain of 10% (Figure S16); Measured radiation patterns of the stretchable 3D and 2D dipole antenna in the E_plane or H_plane (Figure S17); Measured received power with the stretchable 3D dipole antenna as the receiver in air or on skin (Figure S18); Simulated S_{11} curves of a stretchable dipole antenna working at ~5 GHz with a reduced dimension (Figure S19); A stretchable wideband dipole antenna cut by a fiber laser on PI/Cu foils (Video S1).

Acknowledgments

This work was supported by the National Science Foundation (NSF) (Grant No. ECCS-1933072), the National Heart, Lung, And Blood Institute of the National Institutes of Health under Award Number R61HL154215, and Penn State University. D.Q. and H.Y. acknowledge the support provided by the International Partnership Program of the Chinese Academy of Science (Grant No.154232KYSB20200016), the Key R & D plan of JiangSu Province (Grant No. BE2021012-1), the National Key Research and Development Program of China (Grant No. 2020YFC2007400). The use of the RF characterization facility provided by Prof. Mehdi Kiani at Penn State University was also acknowledged. Computations for this research were performed on the Pennsylvania State University's Institute for Computational and Data Sciences' Roar supercomputer. J.Z. would like to acknowledge the Leighton Riess Graduate Fellowship and Diefenderfer Graduate Fellowship in Engineering at Penn State University.

References:

1. Xie, Z.; Avila, R.; Huang, Y.; Rogers, J. A., Flexible and Stretchable Antennas for Biointegrated Electronics. *Advanced Materials* **2020,** *32* (15), 1902767.
2. Zhu, J.; Cheng, H., Recent Development of Flexible and Stretchable Antennas for Bio-Integrated Electronics. *Sensors* **2018,** *18* (12), 4364.
3. Kim, J.; Banks, A.; Cheng, H.; Xie, Z.; Xu, S.; Jang, K.-I.; Lee, J. W.; Liu, Z.; Gutruf, P.; Huang, X.; Wei, P.; Liu, F.; Li, K.; Dalal, M.; Ghaffari, R.; Feng, X.; Huang, Y.; Gupta, S.; Paik, U.; Rogers, J. A., Epidermal Electronics with Advanced Capabilities in Near-Field Communication. *Small* **2015,** *11* (8), 906-912.
4. Lin, R.; Kim, H.-J.; Achavananthadith, S.; Kurt, S. A.; Tan, S. C. C.; Yao, H.; Tee, B. C. K.; Lee, J. K. W.; Ho, J. S., Wireless battery-free body sensor networks using near-field-enabled clothing. *Nature Communications* **2020,** *11* (1), 444.
5. Huang, X.; Liu, Y.; Cheng, H.; Shin, W.-J.; Fan, J. A.; Liu, Z.; Lu, C.-J.; Kong, G.-W.; Chen, K.; Patnaik, D.; Lee, S.-H.; Hage-Ali, S.; Huang, Y.; Rogers, J. A., Materials and Designs for Wireless Epidermal Sensors of Hydration and Strain. *Advanced Functional Materials* **2014,** *24* (25), 3846-3854.
6. Keum, D. H.; Kim, S.-K.; Koo, J.; Lee, G.-H.; Jeon, C.; Mok, J. W.; Mun, B. H.; Lee, K. J.; Kamrani, E.; Joo, C.-K.; Shin, S.; Sim, J.-Y.; Myung, D.; Yun, S. H.; Bao, Z.; Hahn, S. K., Wireless smart contact lens for diabetic diagnosis and therapy. *Science Advances* **2020,** *6* (17), eaba3252.
7. Shin, G.; Gomez, A. M.; Al-Hasani, R.; Jeong, Y. R.; Kim, J.; Xie, Z.; Banks, A.; Lee, S. M.; Han, S. Y.; Yoo, C. J.; Lee, J.-L.; Lee, S. H.; Kurniawan, J.; Tureb, J.; Guo, Z.; Yoon, J.; Park, S.-I.; Bang, S. Y.; Nam, Y.; Walicki, M. C.; Samineni, V. K.; Mickle, A. D.; Lee, K.; Heo, S. Y.; McCall, J. G.; Pan, T.; Wang, L.; Feng, X.; Kim, T.-i.; Kim, J. K.; Li, Y.; Huang, Y.; Gereau, R. W.; Ha, J. S.; Bruchas, M. R.; Rogers, J. A., Flexible Near-Field Wireless Optoelectronics as Subdermal Implants for Broad Applications in Optogenetics. *Neuron* **2017,** *93* (3), 509-521.e3.
8. Liu, J.; Liu, Z.; Li, X.; Zhu, L.; Xu, G.; Chen, Z.; Cheng, C.; Lu, Y.; Liu, Q., Wireless, battery-free and wearable device for electrically controlled drug delivery: sodium salicylate released from bilayer polypyrrole by near-field communication on smartphone. *Biomedical Microdevices* **2020,** *22* (3), 53.
9. Xu, G.; Lu, Y.; Cheng, C.; Li, X.; Xu, J.; Liu, Z.; Liu, J.; Liu, G.; Shi, Z.; Chen, Z.; Zhang, F.; Jia, Y.; Xu, D.; Yuan, W.; Cui, Z.; Low, S. S.; Liu, Q., Battery-Free and Wireless Smart Wound Dressing for Wound Infection Monitoring and Electrically Controlled On-Demand Drug Delivery. *Advanced Functional Materials* **2021,** 31, 2100852.
10. Gil, I.; Fernández-García, R.; Tornero, J. A., Embroidery manufacturing techniques for textile dipole antenna applied to wireless body area network. *Textile Research Journal* **2018,** *89* (8), 1573-1581.
11. Paraskevopoulos, A.; Fonseca, D. d. S.; Seager, R. D.; Whittow, W. G.; Vardaxoglou, J. C.; Alexandridis, A. A. Higher-mode textile patch antenna with embroidered vias for on-body communication *IET Microwaves, Antennas & Propagation* , 2016, p. 802-807.
12. Song, L.; Myers, A. C.; Adams, J. J.; Zhu, Y., Stretchable and Reversibly Deformable Radio Frequency Antennas Based on Silver Nanowires. *ACS Applied Materials & Interfaces* **2014,** *6* (6), 4248-4253.
13. Huang, X.; Leng, T.; Zhu, M.; Zhang, X.; Chen, J.; Chang, K.; Aqeeli, M.; Geim, A. K.; Novoselov, K. S.; Hu, Z., Highly Flexible and Conductive Printed Graphene for Wireless Wearable Communications Applications. *Scientific Reports* **2015,** *5* (1), 18298.
14. Zandvakili, M.; Honari, M. M.; Mousavi, P.; Sameoto, D., Gecko-Gaskets for Multilayer, Complex, and Stretchable Liquid Metal Microwave Circuits and Antennas. *Advanced Materials Technologies* **2017,** *2* (11), 1700144.
15. Guo, R.; Tang, J.; Dong, S.; Lin, J.; Wang, H.; Liu, J.; Rao, W., One-Step Liquid Metal Transfer Printing: Toward Fabrication of Flexible Electronics on Wide Range of Substrates. *Advanced Materials Technologies* **2018,** *3* (12), 1800265.

16. Kwon, K. Y.; Truong, V. K.; Krisnadi, F.; Im, S.; Ma, J.; Mehrabian, N.; Kim, T.-i.; Dickey, M. D., Surface Modification of Gallium-Based Liquid Metals: Mechanisms and Applications in Biomedical Sensors and Soft Actuators. *Advanced Intelligent Systems* **2020,** *3:*2000159.
17. Zhu, J.; Fox, J. J.; Yi, N.; Cheng, H., Structural Design for Stretchable Microstrip Antennas. *ACS Applied Materials & Interfaces* **2019,** *11* (9), 8867-8877.
18. Zhu, J.; Hu, Z.; Song, C.; Yi, N.; Yu, Z.; Liu, Z.; Liu, S.; Wang, M.; Dexheimer, M. G.; Yang, J.; Cheng, H., Stretchable wideband dipole antennas and rectennas for RF energy harvesting. *Materials Today Physics* **2021,** *18*, 100377.
19. Zhu, J.; Zhang, S.; Yi, N.; Song, C.; Qiu, D.; Hu, Z.; Li, B.; Xing, C.; Yang, H.; Wang, Q.; Cheng, H., Strain-Insensitive Hierarchically Structured Stretchable Microstrip Antennas for Robust Wireless Communication. *Nano-Micro Letters* **2021,** *13* (1), 108.
20. Kim, Y.-S.; Basir, A.; Herbert, R.; Kim, J.; Yoo, H.; Yeo, W.-H., Soft Materials, Stretchable Mechanics, and Optimized Designs for Body-Wearable Compliant Antennas. *ACS Applied Materials & Interfaces* **2020,** *12* (2), 3059-3067.
21. Chang, T.; Tanabe, Y.; Wojcik, C. C.; Barksdale, A. C.; Doshay, S.; Dong, Z.; Liu, H.; Zhang, M.; Chen, Y.; Su, Y.; Lee, T. H.; Ho, J. S.; Fan, J. A., A General Strategy for Stretchable Microwave Antenna Systems using Serpentine Mesh Layouts. *Advanced Functional Materials* **2017,** *27* (46), 1703059.
22. Mendes, C.; Peixeiro, C., On-Body Transmission Performance of a Novel Dual-Mode Wearable Microstrip Antenna. *IEEE Transactions on Antennas and Propagation* **2018,** *66* (9), 4872-4877.
23. Yan, Z.; Pan, T.; Yao, G.; Liao, F.; Huang, Z.; Zhang, H.; Gao, M.; Zhang, Y.; Lin, Y., Highly stretchable and shape-controllable three-dimensional antenna fabricated by "Cut-Transfer-Release" method. *Scientific Reports* **2017,** *7* (1), 42227.
24. Liu, F.; Cheng, X.; Zhang, F.; Chen, Y.; Song, H.; Huang, Y.; Zhang, Y., Design and Assembly of Reconfigurable 3D Radio-Frequency Antennas Based on Mechanically Triggered Switches. *Advanced Electronic Materials* **2019,** *5* (6), 1900256.
25. Magill, M. K.; Conway, G. A.; Scanlon, W. G., Tissue-Independent Implantable Antenna for In-Body Communications at 2.36–2.5 GHz. *IEEE Transactions on Antennas and Propagation* **2017,** *65* (9), 4406-4417.
26. Sareni, B.; Krähenbühl, L.; Beroual, A.; Brosseau, C., Effective dielectric constant of random composite materials. *Journal of Applied Physics* **1997,** *81* (5), 2375-2383.
27. Hussain, A. M.; Ghaffar, F. A.; Park, S. I.; Rogers, J. A.; Shamim, A.; Hussain, M. M., Metal/Polymer Based Stretchable Antenna for Constant Frequency Far-Field Communication in Wearable Electronics. *Advanced Functional Materials* **2015,** *25* (42), 6565-6575.

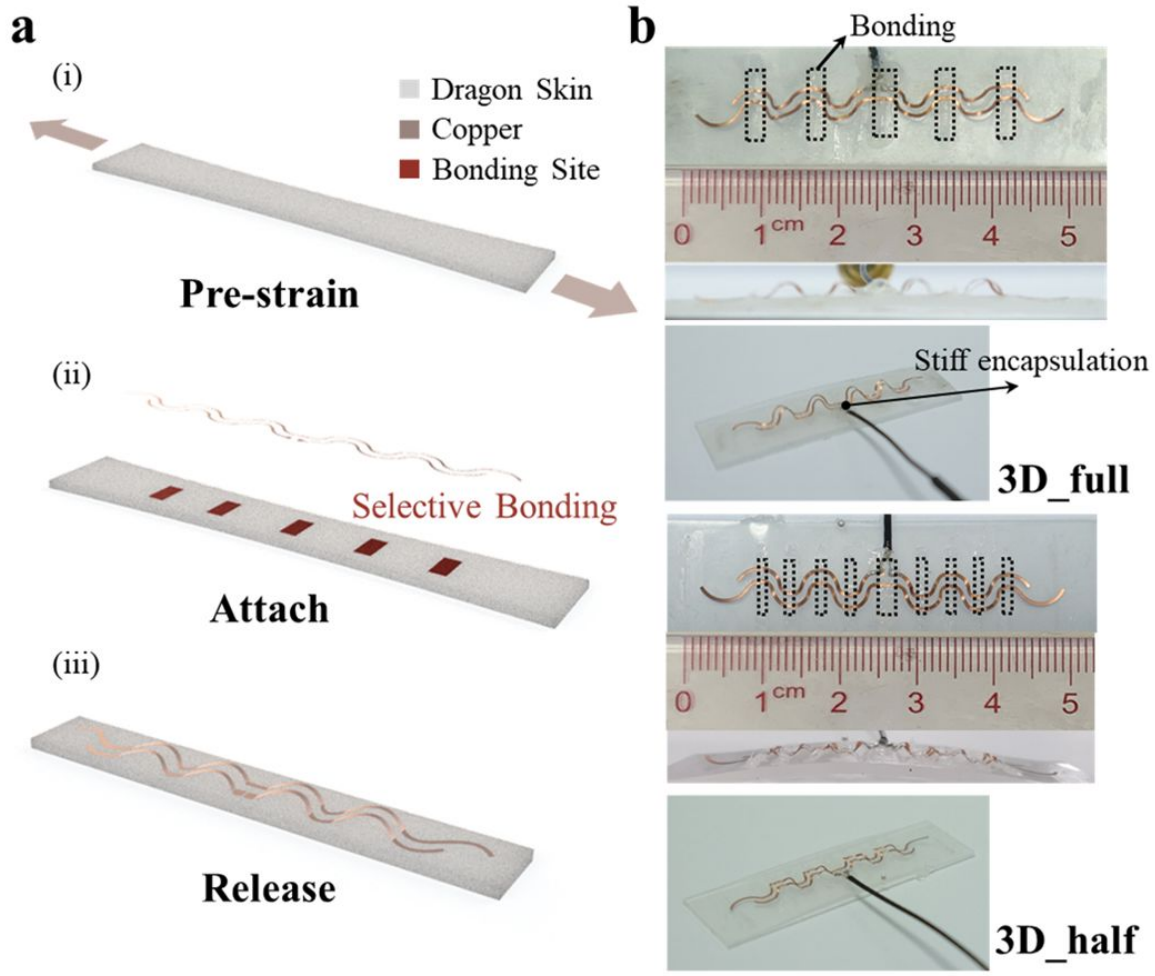

Figure 1. Mechanical assembly of 3D dipole antennas. **a.** Fabrication process of the 3D dipole antenna from the mechanical assembly. **(i)** After the soft Dragon Skin substrate is pre-stretched, **(ii)** the 2D dipole antenna fabricated by laser cutting is attached to the pre-stretched substrate with selective bonding sites. **(iii)** Release of the pre-strain lifts the non-bonded region to form a 3D structure. **b.** Optical images of two representative 3D dipole antennas (i.e., the "3D_full" and "3D_half" dipole antenna) with different configurations by changing bonding sites.

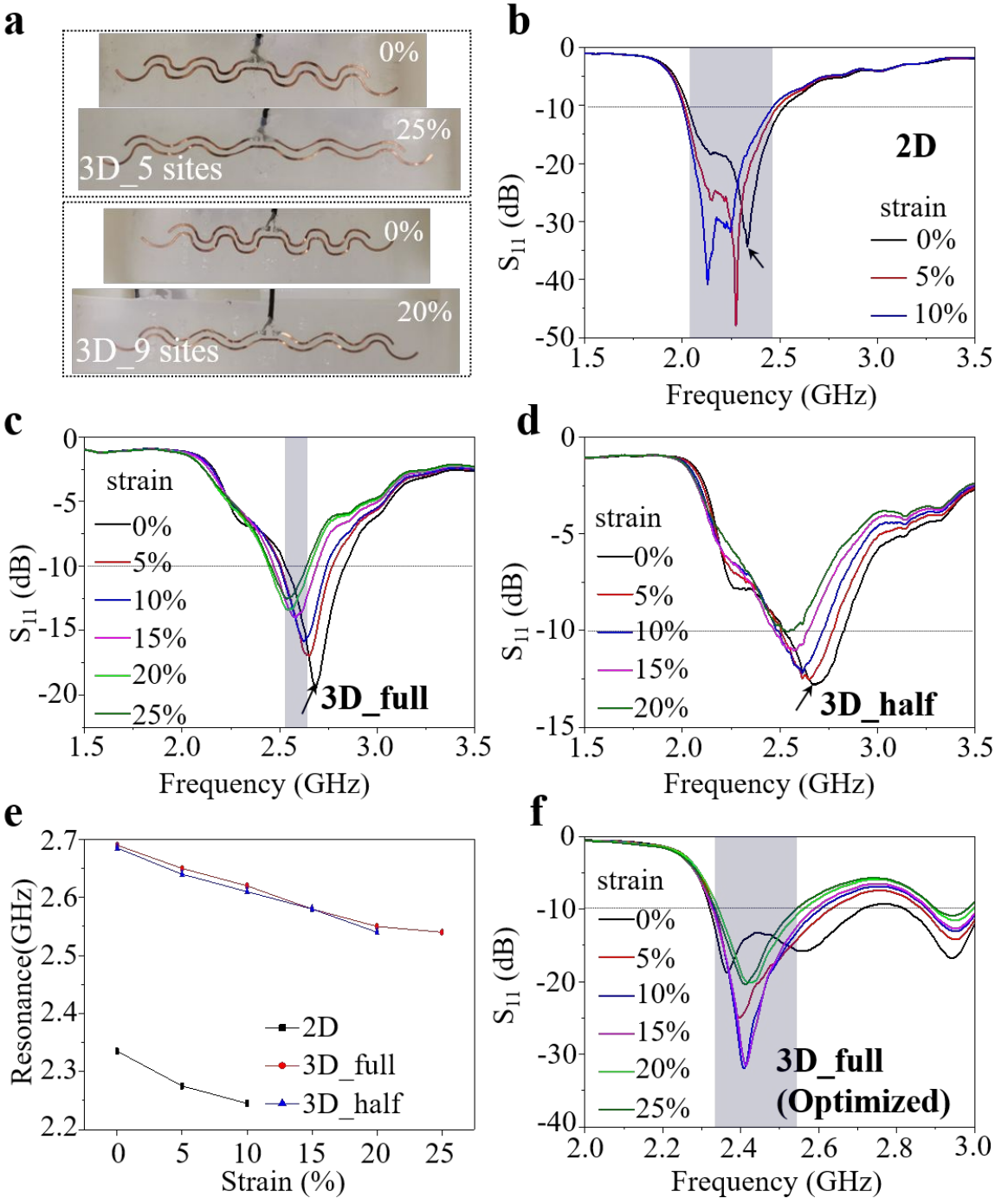

Figure 2. Mechanical-electromagnetic properties of the 2D and 3D stretchable dipole antenna. a. Optical image of the 3D dipole antennas ("3D_full" and "3D_half") upon stretching. **b-d.** S_{11} curves of the dipole antenna upon different stretching. The higher resonant frequency from the short arm was marked by arrows. The marked region highlights the operational band of

the dipole antenna upon stretching. **e.** The higher resonant frequency as a function of stretching. **f.** S_{11} curves of the optimized "3D_full" dipole antenna with the target frequency (2.45 GHz) covered upon stretching.

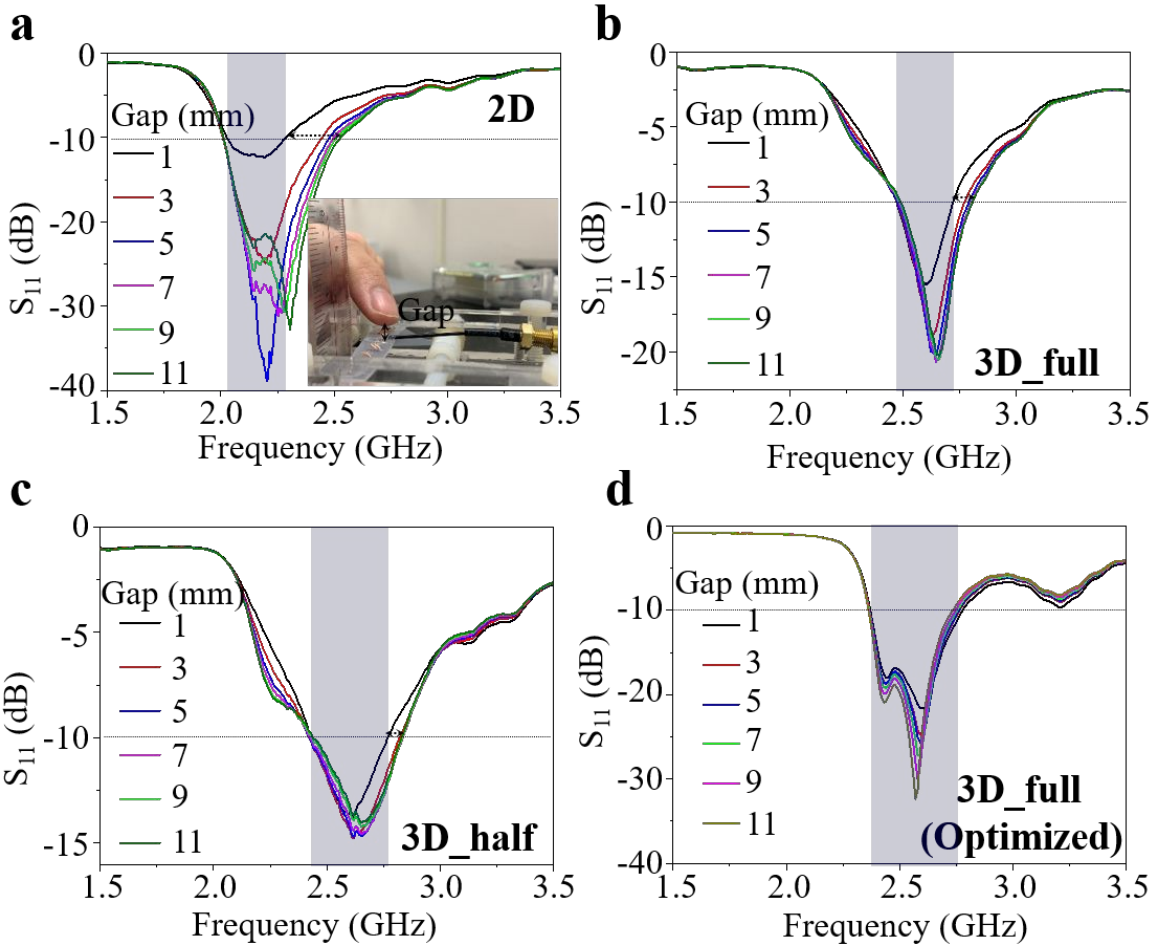

Figure 3. On-body radiation performance of the 2D and 3D dipole antenna. a. Experimental setups for measurements of the on-body radiation performance. S_{11} curves of the 2D (**b**), "3D_full" (**c**), and "3D_half" (**d**) dipole antenna with a fingertip place on the top with different distances.

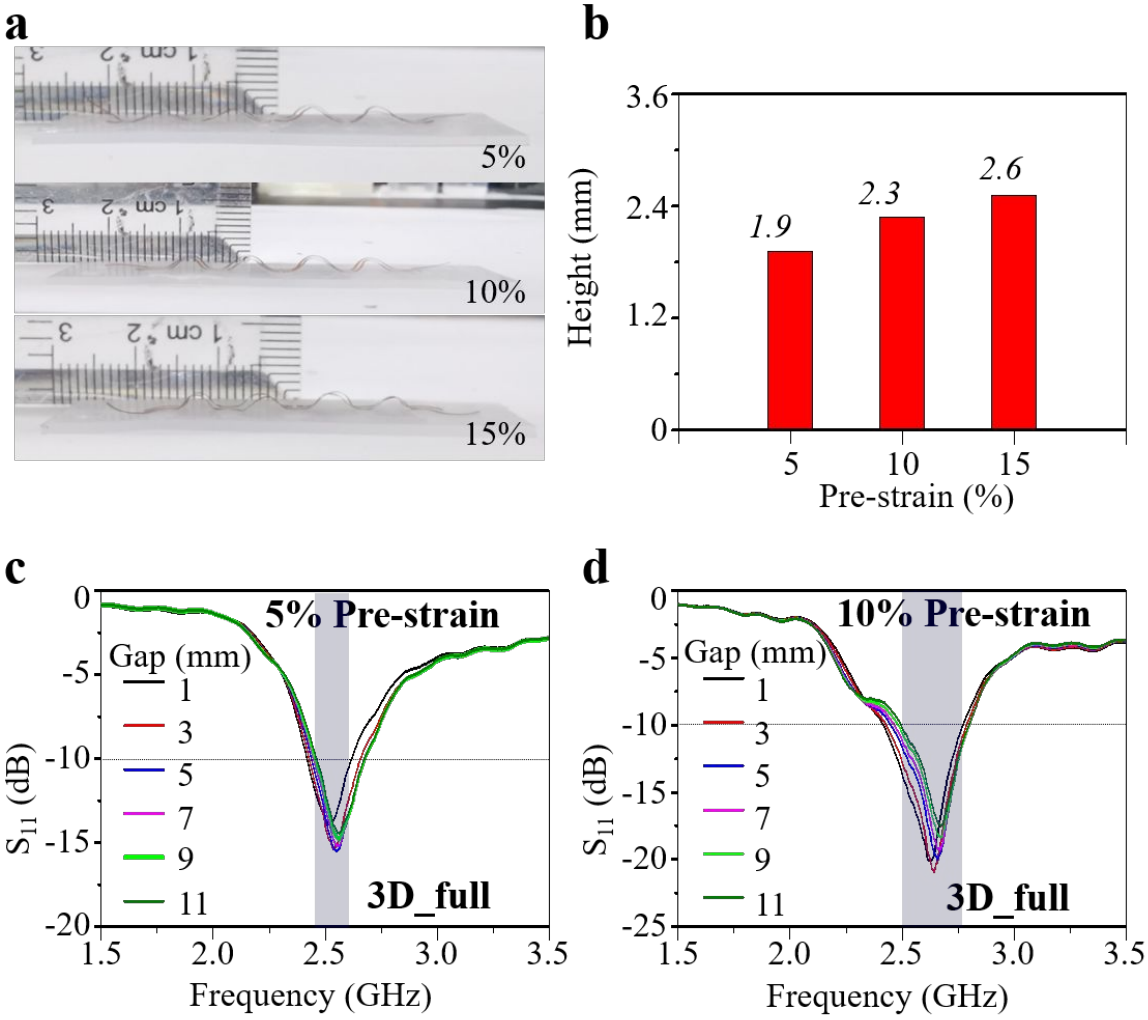

Figure 4. Influence of pre-strain in the mechanical assembly on the on-body radiation performance of the "3D_full" dipole antenna. a. Optical images of the "3D_full" dipole antenna induced by different pre-strain. **b.** The measured arch height as a function of pre-strain. Measured S_{11} curves of the "3D_full" dipole antenna induced by a 5% (**c**) or 10 % (**d**) pre-strain with different distances to a fingertip.

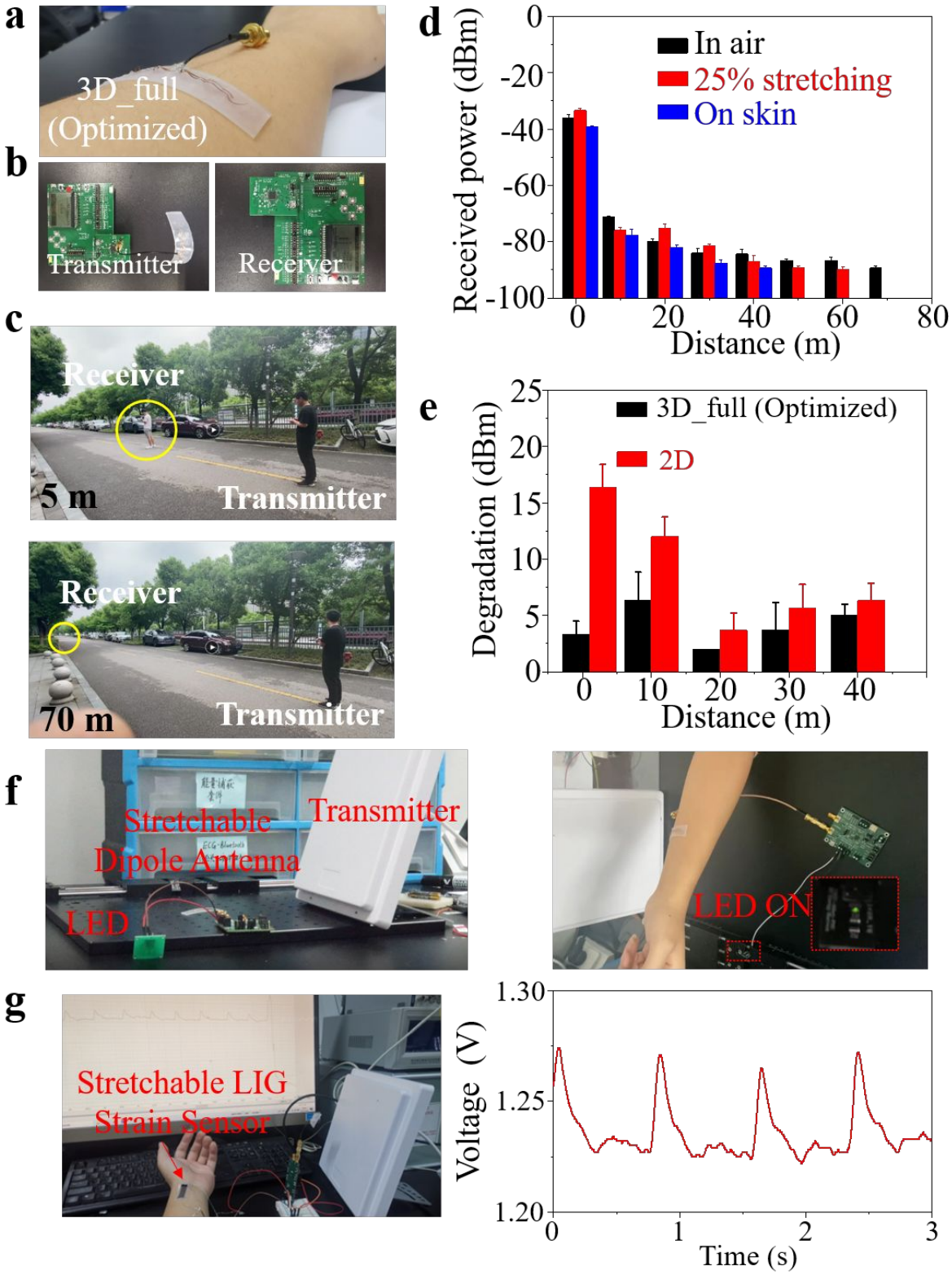
a
3D_full
(Optimized)
b
Transmitter
Receiver
c
Receiver
5 m
Transmitter
Receiver
70 m
Transmitter
d
Received power (dBm)
0
-20
-40
-60
-80
-100
0
20
40
60
80
Distance (m)
In air
25% stretching
On skin
e
Degradation (dBm)
25
20
15
10
5
0
0
10
20
30
40
Distance (m)
3D_full (Optimized)
2D
f
Stretchable
Dipole Antenna
Transmitter
LED
LED ON
g
Stretchable LIG
Strain Sensor
Voltage (V)
1.30
1.25
1.20
0
1
2
3
Time (s)

Figure 5. On-body wireless communication and energy harvesting performance of the "3D_full (Optimized)" dipole antenna. **a.** Optical images of the "3D_full" dipole antenna conformally attached to human arms. **b.** Optical images of the transmitter and receiver used for the evaluation of wireless communication performance. **c.** The experimental setup to evaluate the on-body wireless communication performance. **d.** Measured received power of the "3D_full (optimized)" dipole antenna in free-space or on the human arm with/without a tensile strain of 25%. **e.** The degradation of wireless communication of the dipole antenna when being attached to human arms. **f.** Demonstration of the RF energy harvesting with the stretchable dipole antenna to power a red light-emitting diode (LED). **g.** Continuous pulse measurement from a healthy human subject with the laser-induced graphene (LIG) strain sensor powered by the harvested RF energy for self-powered strain sensing.

TOC

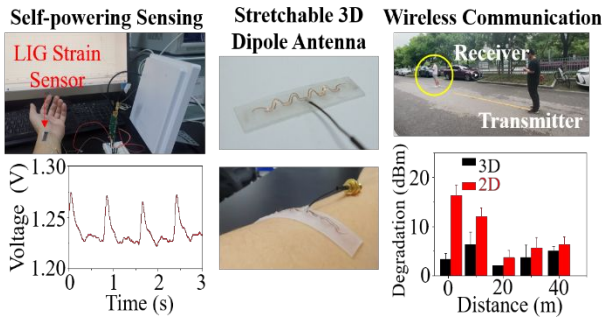
Self-powering Sensing
LIG Strain Sensor
Stretchable 3D Dipole Antenna
Wireless Communication
Receiver
Transmitter
Voltage (V)
1.30
1.25
1.20
0
1
2
3
Time (s)
Degradation (dBm)
3D
2D
20
10
0
0
20
40
Distance (m)